A FULLY DISTRIBUTED STRAIN ROSETTE USING HIGH DEFINITION FIBER OPTIC SENSING

Elias D. Bearinger, Dan Kominsky, Reginald L. Bryson, Nur Aida Abdul Rahim

Luna Innovations Inc.
Blacksburg, VA

ABSTRACT

Integration of new materials into critical structures and applications has driven the need for using strain profiles to characterize material behavior, conduct structural health monitoring, and enable in-situ non-destructive evaluation to drive condition-based maintenance. Due to their small size, flexibility, and low weight, High-Definition Fiber Optic Sensors (HD-FOS) have been frequently utilized for highly spatially-resolved strain measurements with a sampling spacing of 0.65 mm on a wide variety of materials and complex part geometries. HD-FOS, like many fiber optic sensors, is primarily sensitive to strain along the length of the fiber, making it impossible to accurately determine principal and shear strains with a single straight sensor. This work demonstrates how a single fiber can be configured into a rosette geometry, allowing planar and shear strains to be fully characterized. New research has shown that by arranging a single fiber optic sensor in an extended rosette pattern, distributed principal strains and their orientations can be determined at any location within the pattern. This research focused on integrating fiber optic sensors into composite structures and culminated with embedding a distributed rosette pattern into a composite helicopter rotor blade. The rotor blade was shown to be effective in measuring distributed strains on the order of ±500 microstrain along its curved surfaces, resulting in a highly-desirable smart structure capable of measuring its own mechanical integrity.

1. INTRODUCTION

In an effort to reduce weight, minimize cost, and improve performance, many industries are incorporating composites and other advanced materials into critical applications that have historically used metals. Even as the advantages of these innovative materials satisfy the above needs, they come with their own set of challenges. Due to the complexity of composite failure mechanisms and the associated difficulty in developing accurate failure prediction models, there is a pressing need to experimentally characterize performance and to monitor the material's mechanical integrity during its operational life [1]. In particular, the ability to determine distributed principal strains would be useful to design engineers for validating models. There are many technologies that are actively used to determine material performance and conduct structural health monitoring (SHM). However, each of these technologies has limitations that prohibit them from addressing the needs of certain industries for a lightweight, embeddable, and high-definition strain measurement.

The rotorcraft industry is one of the markets in which traditional methods have failed to address the evolving needs for complex structural health monitoring in composite parts. Rotorcraft blades are increasingly made primarily from composite materials. One promising avenue to improving

SAMPE Conference Proceedings. Charlotte, NC, May 20-23, 2019. Society for the Advancement of Material and Process Engineering – North America.

safety and reliability would be the ability to monitor these critical structures for defects, so that blades can be repaired or replaced prior to a catastrophic failure. Methods currently in use to monitor blades for defect formation and growth include visual/tactile inspection, digital image correlation (DIC), and ultrasonic testing. Visual and tactile inspection is highly operator-dependent, potentially incomprehensive, and prone to missing defects that are not visible on the part surface. DIC can offer good distributed surface strain mapping, but it is inherently not embeddable and requires a line of sight from the camera and a proper and repeatable setup if used in the field. Additionally, DIC can be sensitive to speckle contamination [2]. Ultrasonic testing can be effective in locating sub-surface defects, but this method of testing is expensive, time-consuming, and its efficacy depends on the structure of the test article [3].

High-Definition Fiber Optic Sensing (HD-FOS) offers a unique, embeddable solution for determining distributed strain profiles, at a 0.65 mm measurement density, in parts that would be difficult to characterize through traditional methods [4, 5]. Optical fibers can be installed during the part manufacturing process and remain embedded for the lifetime of the component. Using a ground-based interrogation system, the optical strain-sensing fiber can be periodically scanned to detect changes in the strain profile across the part. Since the optical fibers themselves are very small, flexible, lightweight, and possess mechanical properties similar to the carbon fibers in the structure, they do not negatively affect the mechanical properties of the specimen being evaluated.

The authors will begin by introducing basic rosette formations using optical fiber and then show how these basic shapes can be extrapolated to form distributed rosettes. HD-FOS can be used both to determine distributed principal strains across a complex geometry through an extended rosette pattern and also for structural health monitoring when embedded in a part. The value of the distributed rosette compared with standard embedded sensors is that the rosette will allow the user to accurately determine the magnitude and direction of the maximum and minimum strains anywhere in the part. In this way, the true strain profile resulting from a defect can be detected and characterized regardless of the location or orientation of the damage. This would be an extension of current applications where continuous, embedded strain sensing provides crucial information about the initiation and growth of mechanical defects [4, 5]. This work culminates with embedding a distributed fiber optic rosette in a helicopter tail rotor blade. The objective of this paper is to provide engineers, scientists, and technicians a new and effective way of testing and analyzing composite parts.

2. BACKGROUND

2.1 Strain Rosette Theory

Measuring principal strains and orientation is often of interest to engineers since these quantities can be used to predict the onset of failure and failure location. The orthogonal principal strains, denoted ε_1 and ε_2, are the measure of the maximum and minimum strains existing in the measurement plane at a given point. The orientation, φ, represents the angular rotation of the maximum and minimum strains from the arbitrary axis along which the strain measurements were taken. A minimum of three independent strain measurements are needed to calculate ε_1, ε_2, and φ. Historically, these measurements have been taken with foil strain gage (FSG) rosettes [6].

The strain state of an infinitesimal cubic element in 3-dimensional space can be fully described with no less than 6 independent strain quantities: 3 normal and 3 shear. To simplify the calculation process, engineers tend to look at the strains on only one face of the 3-dimensional element. This 2-dimensional view of the strains acting on the cuboid is referred to as the state of plane strain and reduces the number of independent strain measurements needed to fully characterize the element to three, as shown below in Figure 1 (a) [7].

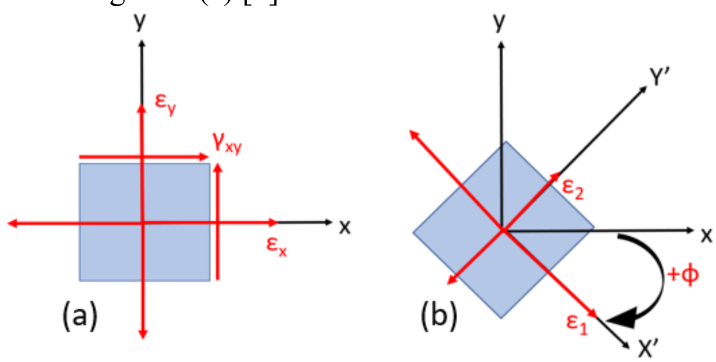

Figure 1. (a) Plane strain element showing normal strains, ε_x and ε_y, and shear strain, γ_{xy}. (b) Plane strain element showing maximum and minimum strains, ε_1 and ε_2, and the orientation, φ.

It is important to keep in mind that the x and y axes are arbitrary relative to the maximum and minimum strain values. However, a new set of axes, x' and y', can be created which do align with the directions of the maximum and minimum strain (principal strains) as shown in Figure 1 (b). Once the element is aligned with the principal strains, the shear strain goes to zero. The two principal strains are perpendicular to each other and offset from the original x/y coordinate system by angle φ. By taking three independent strain measurements around a point of interest, the principal strains, ε_1 and ε_2, and the orientation angle, φ, can be calculated [6, 7].

2.2 High Definition Fiber Optic Sensing (HD-FOS)

The key technology that has enabled this research is high-definition fiber optic sensing (HD-FOS). HD-FOS uses optical frequency domain reflectometry (OFDR) to turn commercially-available optical fiber into a distributed sensor capable of measuring strain or temperature every 0.65 mm along its length. A typical optical fiber used for this type of sensing application is a single-mode fiber consisting of three layers. A germanium-doped fused silica core is surrounded by a pure fused silica cladding. The core/cladding strand is often coated with a polymer (acrylate or polyimide) to improve handleability. A difference in the refractive index between the core and the cladding produces the total internal reflection condition on which fiber optics is based [8].

During the fiber manufacturing process, minute inhomogeneities are inherently introduced along the length of the fiber. These slight variations in refractive index create a random back-reflection fingerprint when the fiber is interrogated using a swept-wavelength laser, through a process known as Rayleigh backscattering. This back-reflection fingerprint is unique to each section of optical fiber and remarkably stable. External stimuli such as strain or temperature causes a distortion in this backscattering pattern of the fiber in a manner proportional to the stimulus being applied.

Luna's Optical Distributed Sensor Interrogator (ODiSI) system takes advantage of the backscatter phenomenon to measure strain and temperature. The process, shown below in Figure 2, begins by detecting the Rayleigh backscatter amplitude profile along the length of the entire sensor (Figure 2 (a)). Next, this backscatter signature is divided into segments called gages. Using an inverse Fourier transform, the data inside this gage-length is converted to the spectral domain as shown in

Figure 2 (b). By running a cross-correlation between the measurement data and a baseline taken at a state of known temperature or strain, a frequency shift in the spectral content of the gage can be observed as shown in Figure 2 (c). This frequency shift corresponds to the distortion of the backscatter signature of the fiber and can be related to either strain or temperature by a set of coefficients [9].

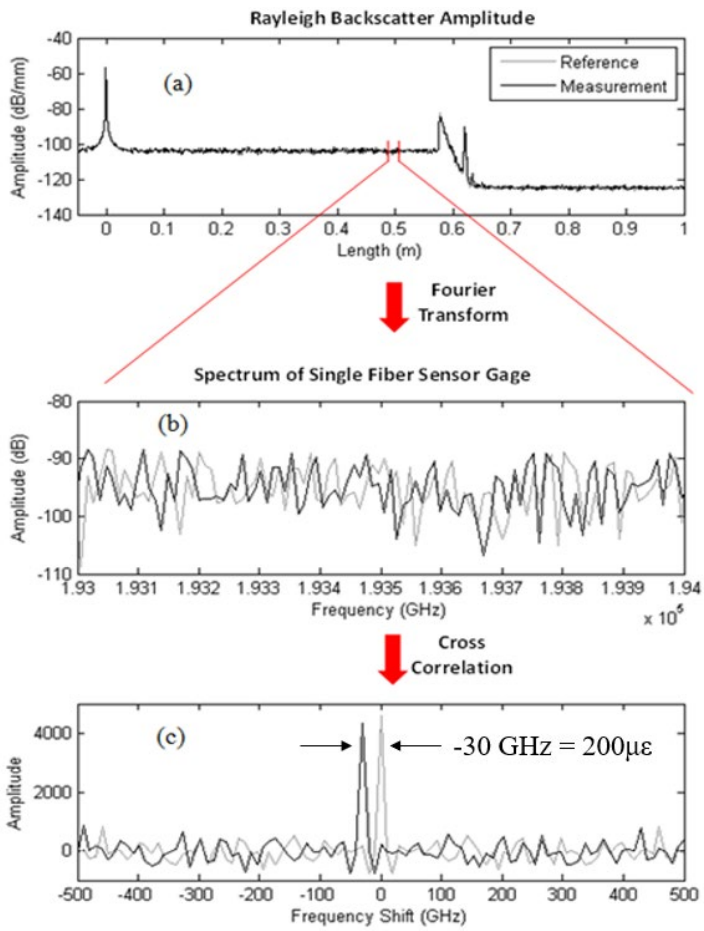

Figure 2. Frequency shift calculation process using Rayleigh backscatter. (a) Backscatter signal amplitude along the length of the sensor. (b) Spectral content of a single gage along the sensor. (c) Cross-correlation giving frequency shift relative to a baseline reference within the gage.

3. EXPERIMENTATION

3.1 Individual Fiber Optic Strain Rosettes

Due to the flexibility and high measurement density along an optical fiber, an infinite number of possible rosette configurations can be created [10]. Two common rosette configurations were installed on 30.5 cm x 4.45cm x 0.32 cm G10 fiberglass coupons, as shown in Figure 3. On each coupon, the rosettes were formed using a single fiber sensor, demonstrating the multiplexing capabilities of HD-FOS. The sections of the fiber shown in solid yellow were bonded to the coupon using M-Bond 200 after the surface was lightly abraded and cleaned. The strains measured by the fiber rosettes were compared with a traditional FSG rosette adhered to the coupon center using AE-15 adhesive and standard installation procedures.

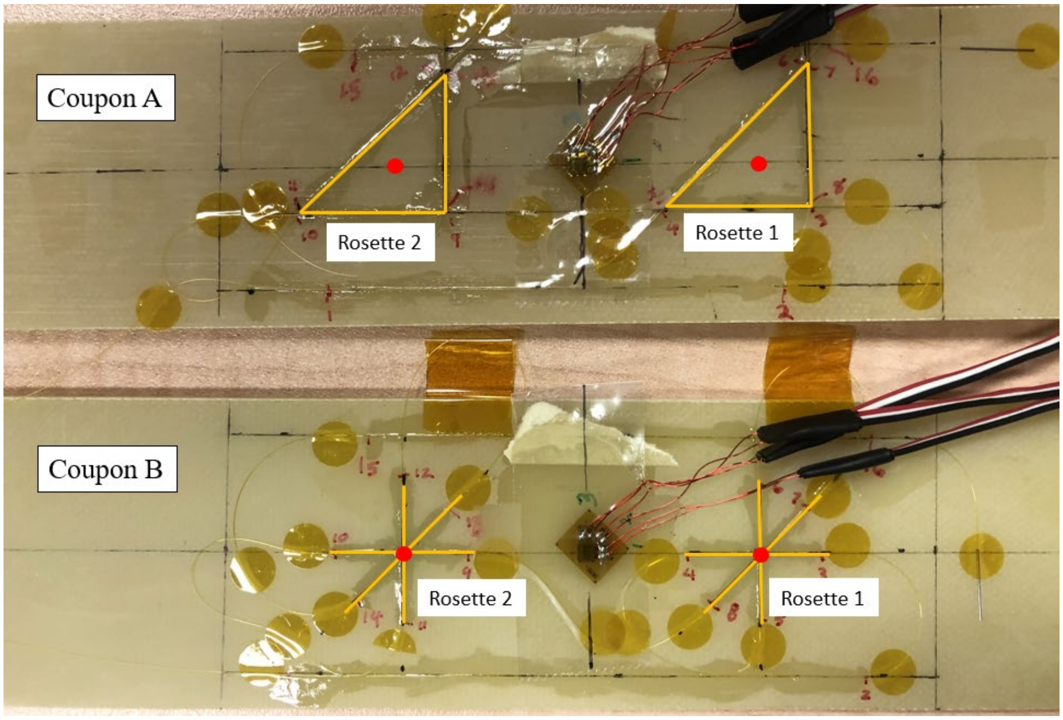

Figure 3. G10 fiberglass coupons instrumented with fiber and foil strain gage rosettes.

The straight sections of each rosette were approximately 2 cm in length, except for the hypotenuse of the triangular rosette on Coupon A, which was slightly longer. The fiber rosettes were each spaced 2.5 cm from the FSG rosette and located such that principal strains measured by each rosette would be located on the centerline of the coupon.

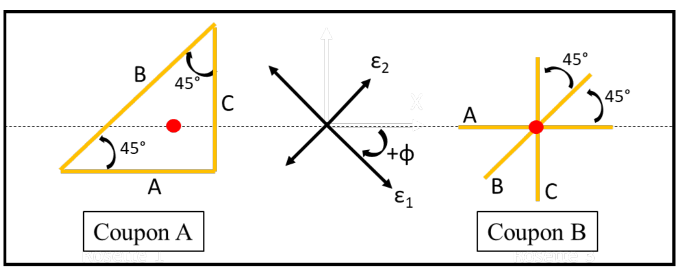

Figure 4. Two different styles of rectangular rosette used for testing.

The rosettes on Coupon A and B are both of the 0-45-90° configuration, which is sometimes called a rectangular rosette [5]. The main difference between these two variations is the spatial relationship of the bonded segments of the rosette to the point of interest, indicated by the red dot in Figure 4. Coupon B has the bonded rosette segments A, B, and C intersecting at the point of interest while on Coupon A the point of interest is located at the centroid of the rosette triangle. One notable consideration is that where the optical fiber crosses over itself, such as at the center of the rosette on Coupon B, the top fiber is spatially separated from the surface of the test article resulting in a possible loss of strain transfer from the test article to the optical fiber.

For both coupons, the measured strain values along segments A, B, and C are averaged to give a single strain value in that direction: ε_A, ε_B, and ε_C, respectively. Using these strain values and Equations 1 and 2 below, the principal strains and the orientation angle, φ, can be calculated [6]. The FSG rosette used for comparison was also of the rectangular rosette configuration and therefore the same equations were used to resolve ε_1, ε_2, and φ from the foil strain gage data.

$$\varepsilon_{1,2} = \frac{\varepsilon_A + \varepsilon_C}{2} \pm \frac{1}{\sqrt{2}}\sqrt{(\varepsilon_A - \varepsilon_B)^2 + (\varepsilon_B - \varepsilon_C)^2} \quad (1)$$

$$\varphi = \frac{1}{2}\tan^{-1}\left(\frac{\varepsilon_A - 2\varepsilon_B + \varepsilon_C}{\varepsilon_A - \varepsilon_C}\right) \quad (2)$$

3.1.1 Fiber Rosette Testing

In order to characterize each of the fiber rosettes, a series of 4-point bend tests were performed on the fiberglass coupons (Figure 5). The 4-point bend test was selected due to its ability to induce a constant strain across the instrumented portion of the coupons. The bend fixture used in these tests had outside contact rollers spaced 26.67 cm apart, with 19.05 cm between the internal contacts which were centered in the fixture. Measurements were zeroed after the top crossmember of the fixture was added and prior to any loads being applied. Increasing loads, ranging from 0 to 9 kg, were applied to the bend fixture as strain data was recorded from both the fiber and the foil strain gage rosettes. Three cycles of the loading regime were repeated for each coupon.

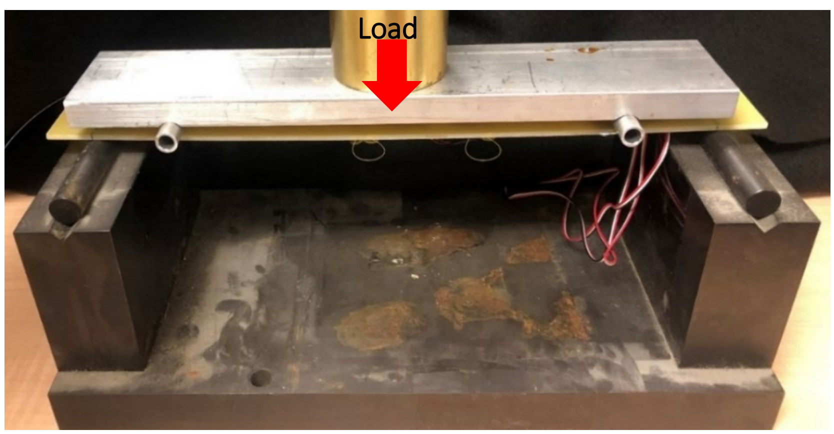

Figure 5. The 4-point bend fixture which was used to load the fiberglass coupons.

3.2 Embedded Distributed Strain Rosette

The individual fiber rosette was then extended to form a distributed lattice of continuous fiber rosette capable of measuring principal strains at many locations across a part. This distributed strain rosette was embedded within a composite rotor blade manufactured by a rotor blade manufacturer. In order to lay out multiple identical fiber rosettes, a repeatable manufacturing process was developed. Additionally, to accurately capture and represent data from these multiple rosettes across a surface with complex curvatures, an extensive measurement and analysis scheme was developed.

3.2.1 Distributed Rosette Layout

It was determined that a modified version of the triangular rosettes used on Coupon A (0-45-90° configuration) would be most conducive to forming a distributed rosette. The pattern chosen is shown in Figure 6 and is formed using a single 10 m high-definition fiber optic sensor. In Figure 6, each of the primary measurement axes are shown in a different color (green [0°], red [45°], or blue [90°]). The manufacturing process for laying out and embedding the sensor is shown in Figure 7.

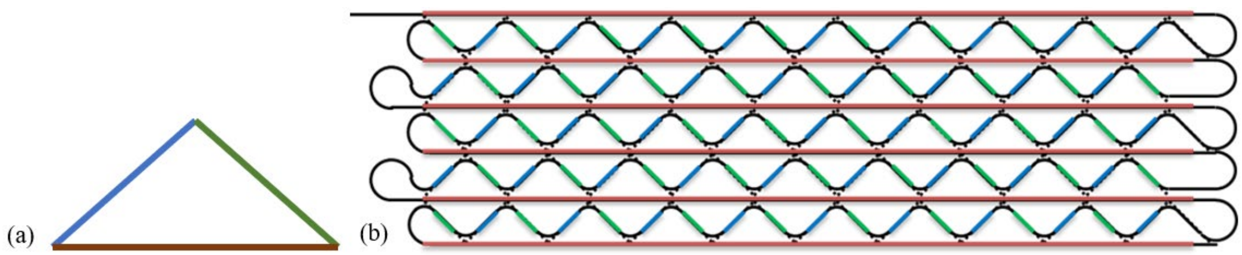

Figure 6. (a) A single 0-45-90° rosette. (b) Distributed 0-45-90° rosette using a single fiber optic strain sensor.

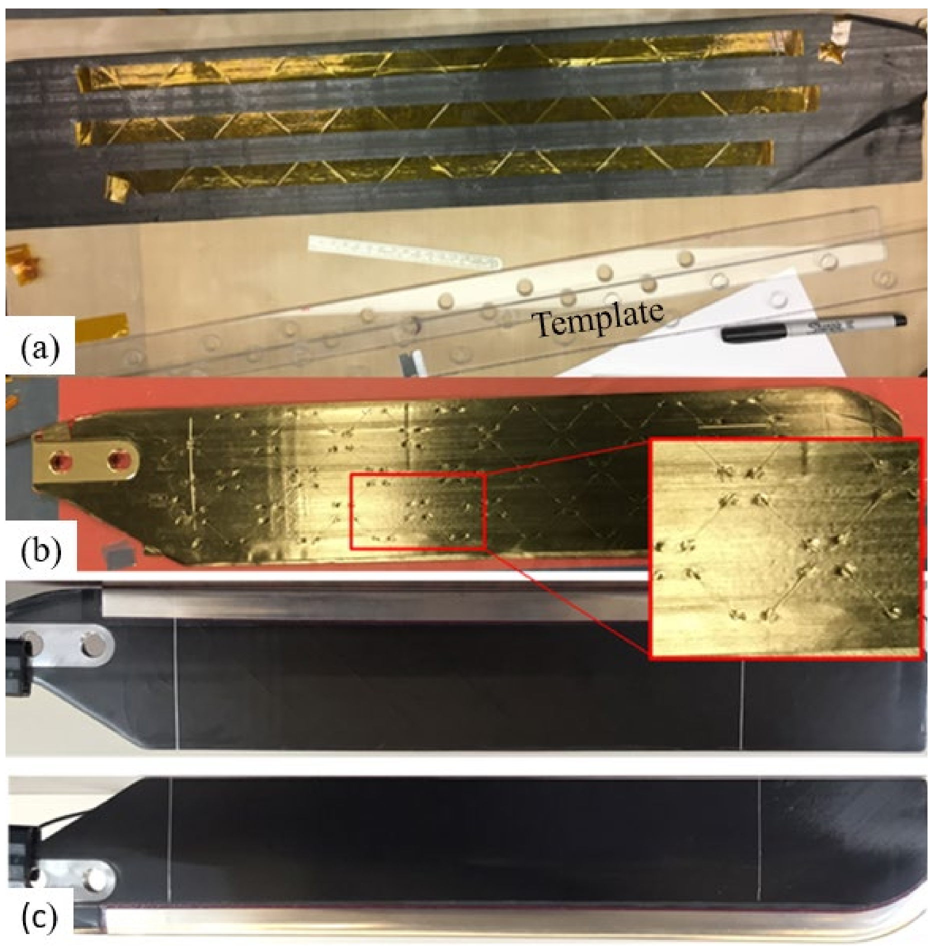

Figure 7. Manufacturing procedure used to incorporate the distributed rosette into a composite tail rotor blade. (a). The template used to form the rosette (bottom) and the rosette installed on the prepreg material. (b) Rosette tacked to prepreg material by localized heating at corners. (c) Finished blade with embedded distributed rosette.

Due to the distributed rosette's complexity and the importance of each segment being oriented correctly, installing the rosettes manually was not a viable option. Instead, a template was used to ensure that the fiber was laid out in the correct orientation and spacing, as seen in Figure 7 (a). From the template, the rosette was transferred to Kapton tape and then to the top sheet of the prepreg material on the mostly-completed blade. The ends of each straight segment were touched with a localized heat source, causing the uniaxial carbon fiber prepreg to become tacky and grip the fiber. This allowed the Kapton tape to be removed while still holding the fiber in the desired layout as shown in Figure 7 (b). A small hole was installed through the foam core close to the trailing edge so that a single fiber could be used to instrument both the high and low pressure sides of the blade. Once the distributed rosette was placed on both sides of the blade, the final prepreg sheet and metal abrasion strip was then installed using the manufacturer's standard process. This resulted in a blade where the embedded rosette is only faintly visible (Figure 7 (c)).

3.2.2 Distributed Rosette Analysis

The challenge with analyzing the distributed rosette was the presence of multiple distinct segments. Each segment needed to be isolated, and the slight manufacturing variations in each had to be captured and taken into account when calculating the resulting strain. A largely automated software program was developed to achieve this. The first step was to isolate the segments based on a photo of the rosette pattern. With minimal user input, the end result was a display of the principal strains and their orientation across a 3D model of the part. This methodology removed the tedious and time-consuming task of analyzing each segment individually. The main steps in the software's algorithm are shown below in Figure 8.

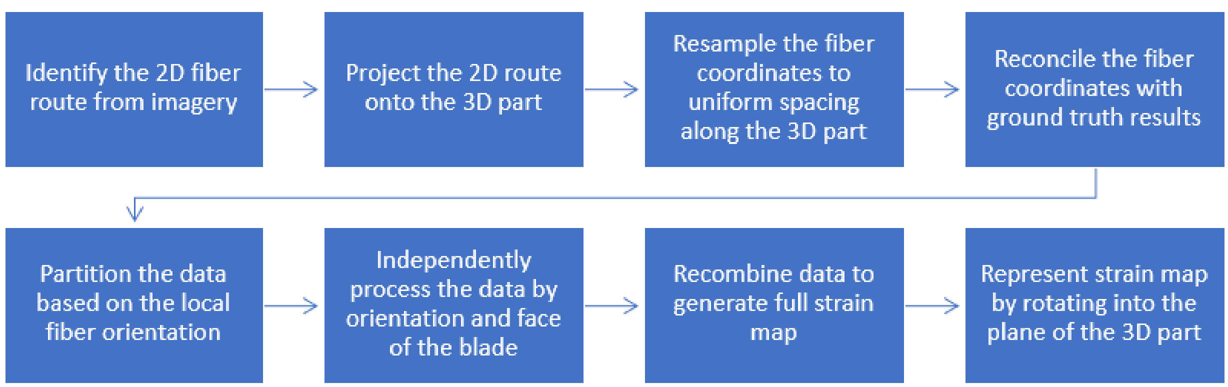

Figure 8. Algorithm used to develop software for plotting principal strains.

4. RESULTS

4.1 Individual Fiber Optic Strain Rosettes

In order to verify the accuracy of distributed fiber strain measurements when laid out in rosette configuration, comparisons were carried out between fiber and FSG rosettes. As the legs of each rosette were laid out in the same direction, a representative plot of fiber strain versus FSG measurement output is shown in Figure 9. This is of fiber Rosette 1 (R1) on coupon A and demonstrates a linear relationship for all 3 leg pairs throughout the loading range. The slope, the zero offset, and the R^2 values are given in Table 1.

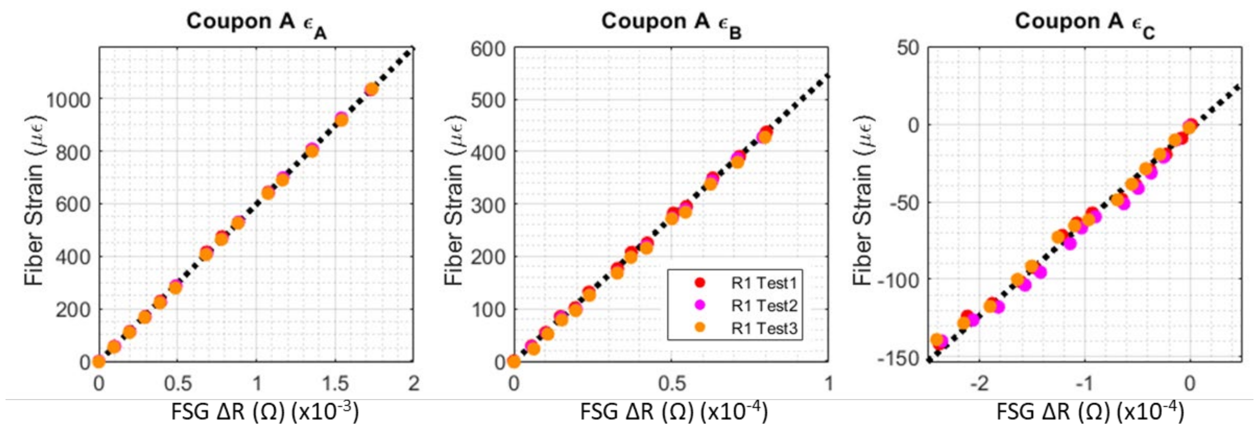

Figure 9. Measurement comparison between each leg of fiber Rosette 1 with the matching FSG rosette leg on Coupon A. The dotted black line indicates a linear trendline.

Table 1. Trendline slope, intercept, and R^2 value, for measurement comparison between each leg of fiber Rosette 1 with the matching FSG rosette leg on Coupon A.

	Slope (x 1e5)	Intercept (με)	R^2
Coupon A; Fiber Rosette ε_1	6.0021	-3.25	0.9999
Coupon A; Fiber Rosette ε_2	5.4797	-2.00	0.9903
Coupon B; Fiber Rosette ε_1	5.7243	-5.68	0.9949

Fiber Rosette 2 on Coupon A was bonded incorrectly (the fiber sensor was lifted off the coupon surface) and measurements from this rosette are not included in the analysis below. Additionally, the FSG on coupon B demonstrated erratic measurements during Test 1, possibly due to an intermittent electrical short in either the gage or the wiring which resulted in faulty readings. and are also not included in the analysis below. For all other rosettes, the principal strains, ε_1 and ε_2, and the orientation angle, φ, were calculated for each rosette on the two coupons. The maximum strain, ε_1, for all tests is positive which is expected since the rosettes were located on the tension face of the bent test article. The minimum strain, ε_2, is negative due to Poisson effects.

The calculated principal strains from the fiber and foil gage rosettes on both coupons were fitted with separate linear trendlines. Importantly, it can be seen that the principal strains calculated from the fiber varies linearly with the FSG (Figure 10). Table 2 shows the slope, the zero offset, the R^2 values, and the root-mean-square-error (RMSE) for both Coupons A and B.

The slopes for all comparisons are very similar, within 0.5% of each other, indicating that the sensors respond repeatably across both coupons. However, the slope value is not 1. This indicates that either the gage factor relating spectral shift in the fiber to strain is incorrect or that the gage factor relating resistance change in the foil rosette to strain is incorrect. The fiber output has been calibrated using a traceable method, as described in [11]. The known sources for foil gage error that are applicable to this test are signal attenuation due to lead wires and the interrogator being out of calibration. The FSG rosettes were hooked up in a two-wire configuration where a four-wire configuration would have taken better account of the lead wire variations. Additionally, the acquisition system was due for re-calibration. These factors could influence the strain output relationship between fiber and FSG. However, the linear relationship between the fiber and foil gage still holds.

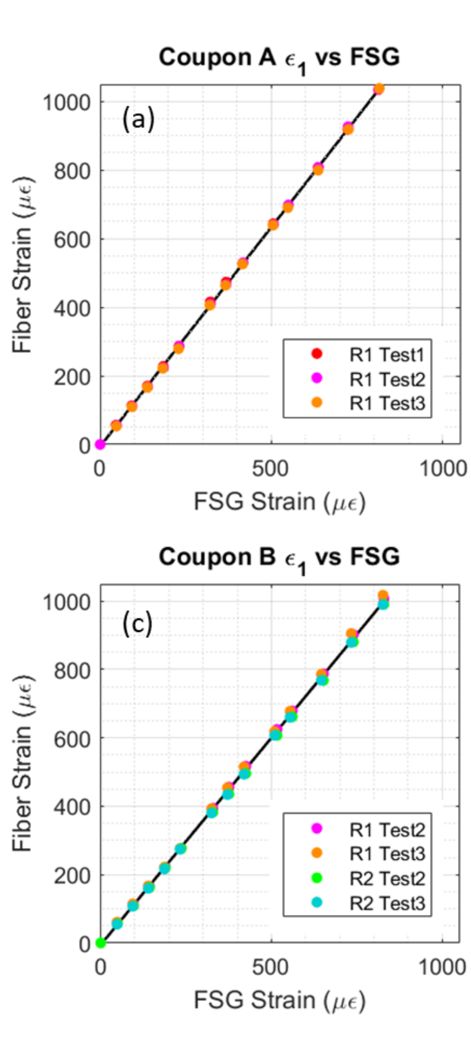

Figure 10. Comparison of the principal strains calculated using the fiber and foil strain gage rosettes throughout the loading range. The black line is a linear fit through the data sets.

Table 2. Trendline slope, intercept, R^2 value, and RMSE for calculated principal strains on Coupons A and B.

	Slope	Intercept (με)	R^2	RMSE (με)
Coupon A; Fiber Rosette ε_1	1.2801	-6.40	0.9998	3.96
Coupon A; Fiber Rosette ε_2	1.2303	-5.29	0.9908	4.09
Coupon B; Fiber Rosette ε_1	1.2116	-5.55	0.9993	8.40
Coupon B; Fiber Rosette ε_2	1.3895	2.55	0.9965	2.62

In addition to determining the value of the maximum and minimum strains on the part, the orientation angle, φ, was calculated. Since the length of the coupon was orthogonal to the applied moment, it was expected that the orientation angle would be 0°. Figure 11 shows that the calculated angle was indeed close to the anticipated value once load was applied. Under the zero-load condition there was no consistent orientation (because there are no principal axes). Under load, the fiber rosettes calculated the direction of the loading with +/- 4° accuracy.

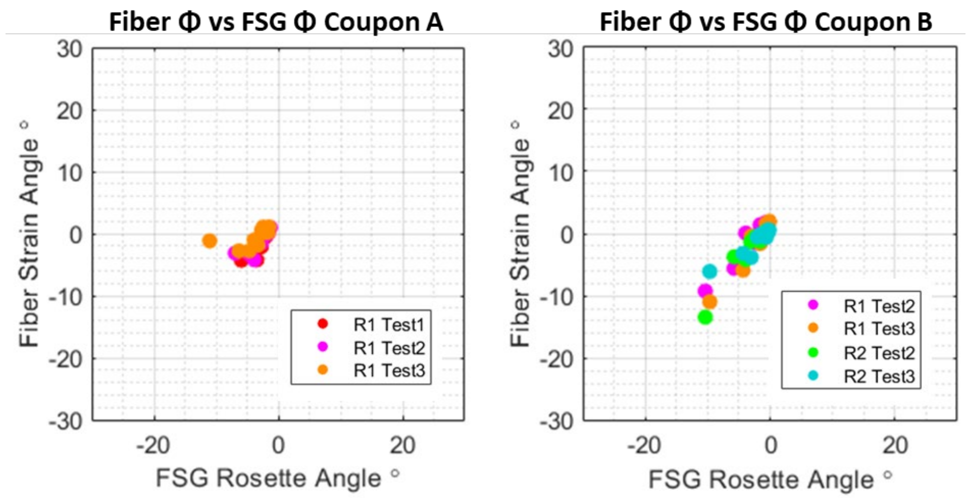

Figure 11. Calculated orientation angle, φ, indicating the angular direction of the maximum strain from the lengthwise axis of the coupon.

4.2 Embedded Distributed Strain Rosette

The next step was to determine the distributed principal strains and orientation angle across both faces of a composite helicopter tail rotor blade during load application. The results shown in Figure 12 to Figure 14 were calculated when the base of the blade (far left) was fixed and the trailing edge (bottom of picture) was lifted, resulting in torsion along the length of the blade. A color map of the strain data as directly measured along the fiber on the suction side of the blade is shown in Figure 12. The three measurement axes are clearly visible, with one axis showing compression, one showing tension, and the horizontal axis showing a strain reading near zero.

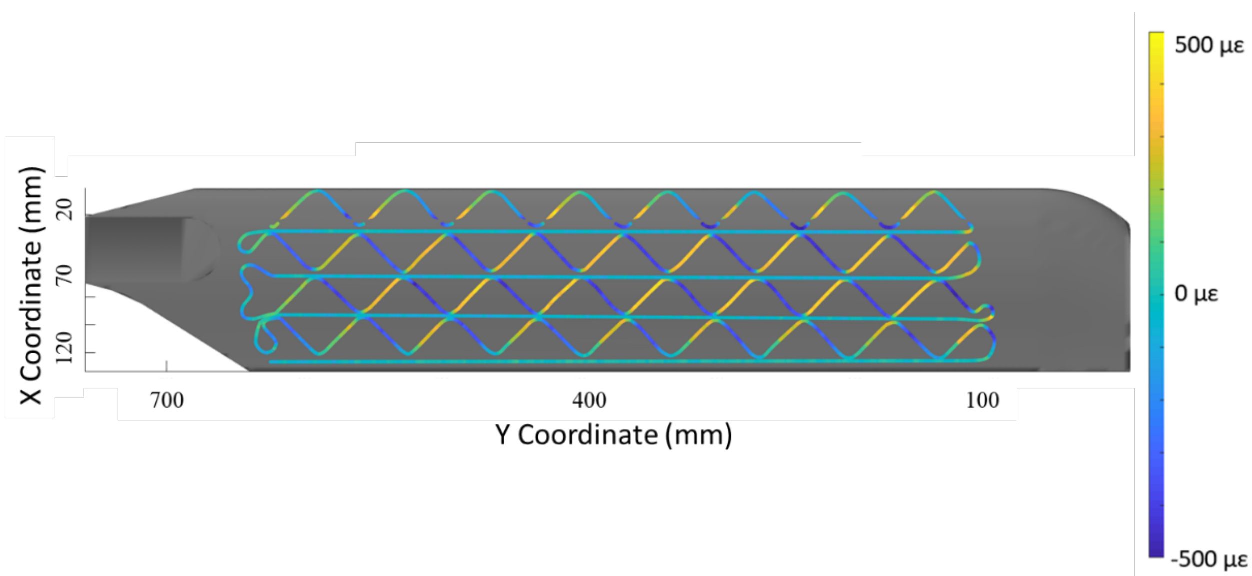

Figure 12. Colormap of strain along distributed rosette located on the suction side of the composite rotor blade

The strain measurements from the suction side of the blade were then separated into each measurement axes. Data from each measurement axis was interpolated across the fiber rosette pattern as shown below in Figure 13. Figure 13 (a) shows the interpolated data from the horizontal measurement axis, while Figure 13 (b) and (c) show the interpolations from the two angled axes.

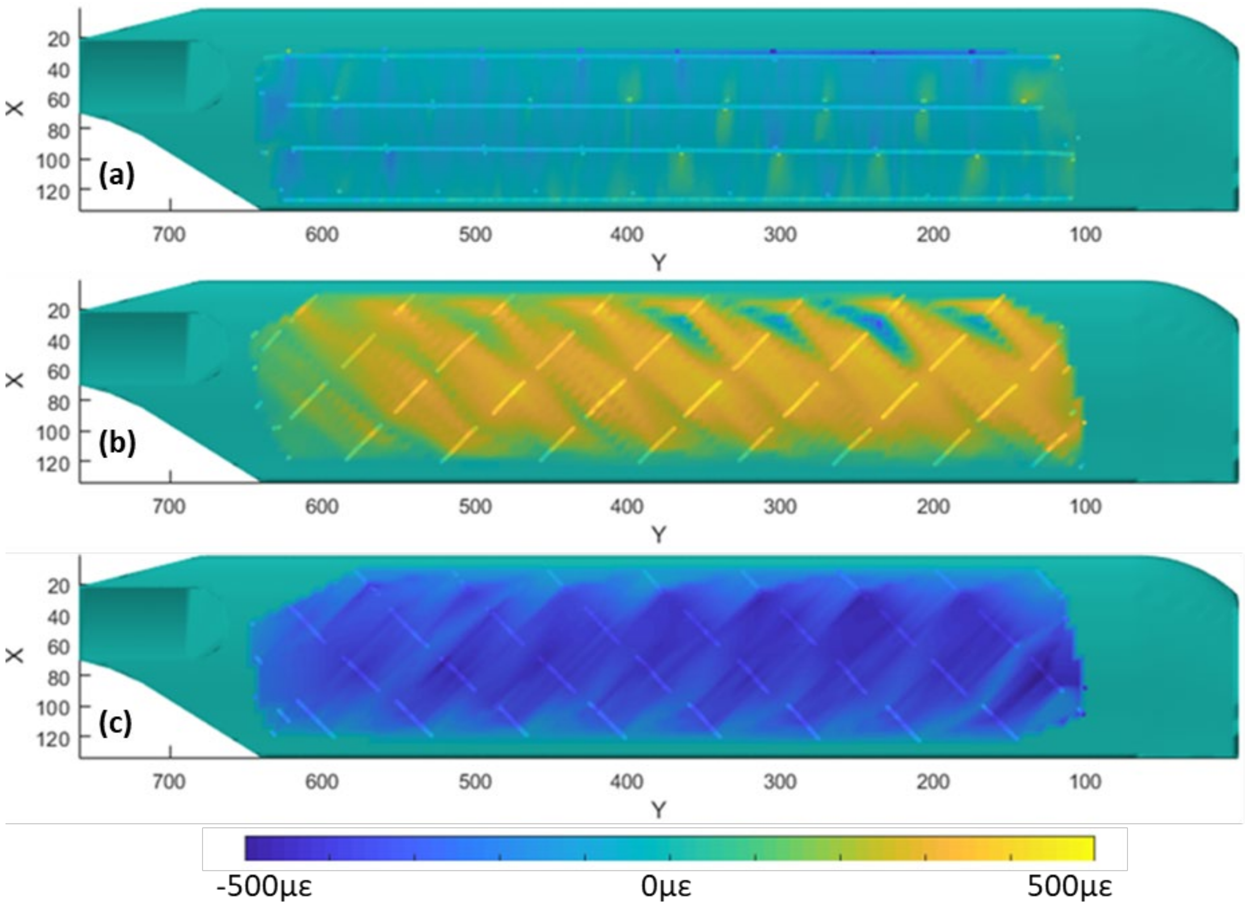

Figure 13. Strain measurements taken using distributed rosette decomposed into three separate measurement axes and interpolated along the blade on the suction side.

Using this distributed map of strain measured along three distinct axes, principal strains and orientation can be calculated at any point along the blade using Equations 1 and 2 as explained previously. The final output of the software is shown in Figure 14, where the distributed principal strains are represented by arrows. The blue (inward pointing) arrows indicate compression and the red (outward pointing) arrows show tension. While these arrow pairs are always perpendicular to each other, their orientation relative to the blade is rotated to describe the angle φ. The length of the arrows describes the relative magnitude of the strain values they represent so that regions of strain concentration can be identified on the part. A similar calculation was carried out for the pressure side of the blade but is not shown here.

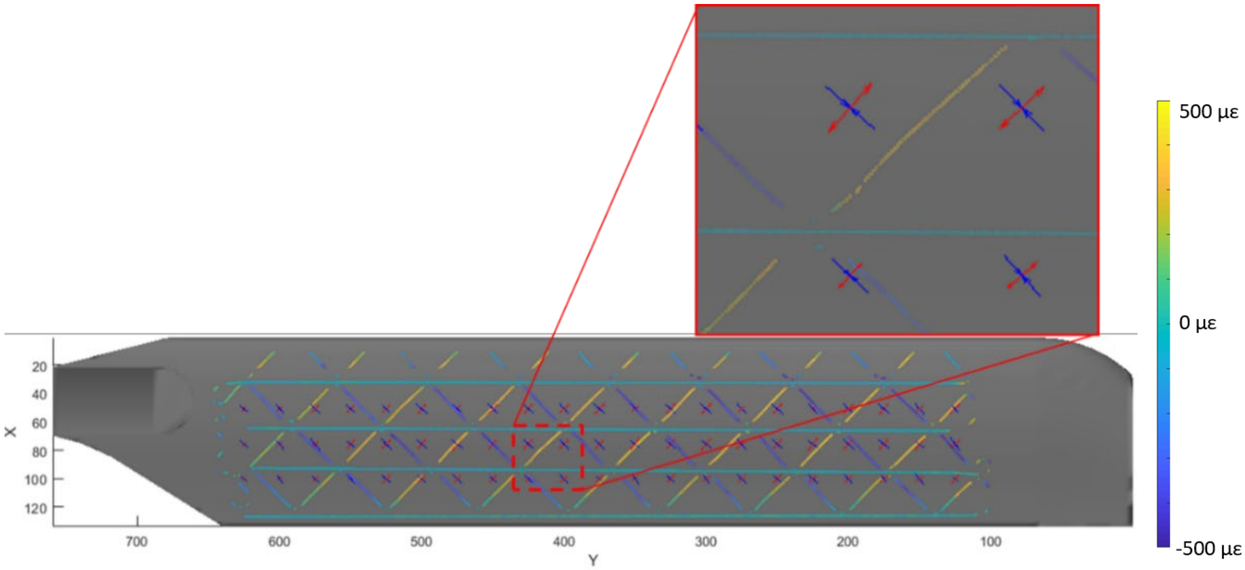

Figure 14. Arrows mapping magnitude and orientation of distributed principal strains across part.

While this technology offers a truly novel method for measuring distributed principal strains and could be tremendously impactful in industry, it does have limitations which should be addressed. It is possible for highly localized strain fluctuations to be inaccurately represented through the interpolation process used in the distributed rosette. As with any measurement of this type, the results will improve in accuracy as the number of rosettes on a given part increases.

While most of this work has focused on the ability to resolve distributed principal strains, the importance of this innovation in structural health monitoring applications should not be underestimated. Damage in critical components may, at times, generate a prominent strain signature in one direction. In past work, optical fiber sensors have been embedded in composite panels and successfully used to detect and localize impact events (Figure 15) [4, 5]. However, since optical fiber is principally sensitive to strain along its length, any fiber configuration besides a rosette used in a structural health monitoring application risks failing to detect damage which generates a strain field perpendicular to its location. For this reason, distributed rosettes afford a promising innovation both for characterizing distributed principal strains and for conducting structural health monitoring.

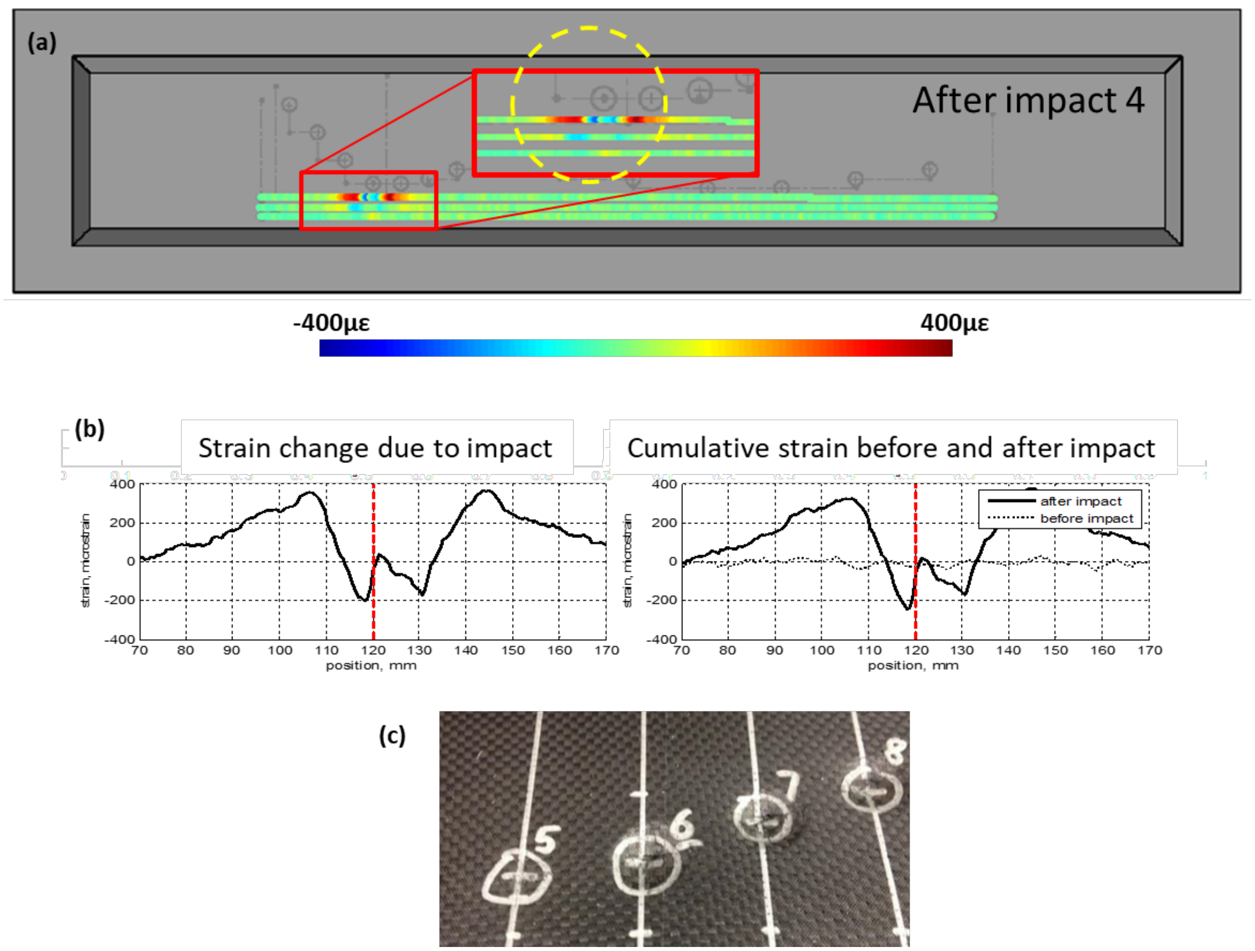

Figure 15: Strain profile along fiber sensors embedded inside a composite panel, after impact damage. (a) Strain along 3 embedded fiber sensors, displayed as a color map on a drawing of the panel after impact. (b) Strain along the top embedded fiber sensor, plotted as both strain change as well as cumulative strain before and after impact, along the sensor length. (c) Photograph of representative impact series on the panel.

5. CONCLUSIONS

In conclusion, this work shows how a single optical fiber can be configured into an extended rosette to measure distributed principal strains and their orientation across an entire test article. Two variants of a 0-45-90° rosette were installed on G10 fiberglass coupons and strained in 4-point bend in order to compare the fiber configurations with foil rosettes, the incumbent technology. Principal strains calculated using data from the optical fiber rosette were shown to have a consistent linear relationship with principal strains calculated using foil strain gage data. A slight difference in slope between strains from the fiber and foil gage on each coupon indicate that gage factors may need to be adjusted to improve agreement and accuracy. A modified version of the 0-45-90° configuration was implemented in the distributed fiber optic rosette which was embedded into a composite rotor blade. Finally, a software program was developed which allowed principal strains to be visualized along a 3D model of the instrumented part with minimal user effort.

Most importantly, this work marks a step towards a new paradigm of non-destructive evaluation, as the information about distributed principal strains on parts instrumented with extended fiber rosettes can be used to conduct structural health monitoring. This technology addresses the pressing need of the rotorcraft industry and other markets as these manufactures strive to make their parts safer, cheaper, and more intelligent.

6. REFERENCES

1. I. M. Daniel, "Failure of Composite Materials under Multi-axial Static and Dynamic Loading," International Symposium on Dynamic Response and Failure of Composite Materials, tech., 2014.
2. Zhu, Y-K., Tian, G-Y., Lu, R-S., and Zhang, H. "A review of optical NDT technologies." *Sensors* 11 (2011): 7773-7798
3. Shull, P. J. *Nondestructive Evaluation: Theory, Techniques, and Applications*. CRC Press; 1st edition, 2002
4. Kominsky, D., Abdul Rahim, N. A., Davis, M. A., Garg, N., Castellucci, M. A., Beaty, N. B. "Damage Detection and Localization in Carbon Fiber Reinforced Polymer Composites using High Definition Fiber Optic Sensors (HD-FOS)." Proceedings of SAMPE 2017. Seattle, WA. May 22-25, 2017
5. Kominsky, D., Abdul Rahim, N. A., Davis, M. A., Garg, N., Castellucci, M. A., Bryson, R. L., Beaty, N. B. "Extracting Information From Damaged Carbon Fiber Composites Using High Definition Fiber Optic Sensing (HD-FOS)." Proceedings of CAMX 2017. Orlando, FL. Dec 12-14, 2017
6. "Strain Transformation and Rosette Gage Theory." [Online]. Available: http://users.tamuk.edu/kfldp00/MEIE_Peel_website/Courses/Meen5330/strain-gage-rosette-theory_GA_Tech.pdf.
7. R. C. Hibbeler, *Mechanics of Materials*, 9th ed. Pearson Prentice Hall.
8. Froggatt, Mark, and Moore, Jason. "High resolution strain measurement in optical fiber with Rayleigh scatter." Appl. Opt. 37 (1998): 1735-1740.
9. Kreger, S., Gifford, D. K., Froggatt, M. E., Soller, B. J., and Wolfe, M. S. "High resolution distributed strain or temperature measurements in single- and multi-mode fiber using swept-wavelength interferometry." *Optical Fiber Sensors, OSA Technical Digest.* Cancun, Mexico, October 23, 2006. Optical Society of America, 2006. Paper ThE42. CD-ROM.
10. D. K. Gifford, M. E. Froggatt, A. K. Sang, and S. T. Kreger, "Multiple fiber loop strain rosettes in a single fiber using high resolution distributed sensing," *Fourth European Workshop on Optical Fibre Sensors*. Vol. 7653. International Society for Optics and Photonics, 2010.
11. "ODiSI-B Sensor Strain Gage Factor Uncertainty". [Online]. Available: https://lunainc.com/wp-content/uploads/2016/01/EN-FY1602-ODiSI-B-Sensor-Strain-Gage-Factor-Uncertainty.pdf